remote sensing

MDPI

Article

The Distribution Characteristics of Large Landslides Along the Daduhe River in the Eastern Tibetan Plateau and Their Effects on Landscape Evolution

Meifang Bian [1], Hengzhi Qiu [2] and Xiaoli Chen [1,*]

[1] Key Laboratory of Earthquake and Volcanic Hazards, Institute of Geology, China Earthquake Administration, Beijing 100029, China; bianmeifang@ies.ac.cn
[2] Zhejiang Earthquake Agency, Hangzhou 310013, China; qiu971007@foxmail.com
* Correspondence: chenxl@ies.ac.cn

Abstract: Landslides play a crucial role in landscape evolution, particularly in tectonically active areas. However, research on the relationship between landslide development and landscape evolution remains limited. This study examines the hypsometric integral (*HI*) values of the Daduhe river mainstem catchments to assess the landscape evolution stage and investigate its spatial correlation with the occurrence of landslides. Additionally, it evaluates the distribution of large landslides concerning elevation and slope. Furthermore, by analyzing the longitudinal profile of the Daduhe river, this study explores the relationship between the occurrence of landslides and knickpoints, as well as the impact of landslides on catchment morphology and material redistribution. The results show that the *HI* values of catchments along the Daduhe river range from 0.35 to 0.71, exhibiting a progression from youth to maturity and monadnock stages from upstream to downstream. Large landslides were predominantly distributed in areas with elevations of 1000–2000 m and slopes < 40°. Their distribution was closely linked to *HI* values: large landslides were sparse in catchments with *HI* > 0.5 (Banma county to Danba county) but more frequent in catchments with *HI* < 0.5 (Danba county to the river outlet). The longitudinal profile of the Daduhe river illustrates variations in channel morphology, with large landslides entering the river and facilitating the formation of knickpoints. The impact of large landslides on catchment landscape transformation, both in terms of morphology and material movement, exhibits a trend of gradual intensification from upstream to downstream. This study shows that landscape evolution can provide rich information to locate regions prone to landslides.

Keywords: Daduhe river; catchments; hypsometric integral; large landslides

check for updates

Academic Editor: Domenico Calcaterra

Received: 10 February 2025
Revised: 20 March 2025
Accepted: 21 March 2025
Published: 22 March 2025

Citation: Bian, M.; Qiu, H.; Chen, X. The Distribution Characteristics of Large Landslides Along the Daduhe River in the Eastern Tibetan Plateau and Their Effects on Landscape Evolution. *Remote Sens.* **2025**, *17*, 1133. https://doi.org/10.3390/rs17071133

Copyright: © 2025 by the authors. Licensee MDPI, Basel, Switzerland. This article is an open access article distributed under the terms and conditions of the Creative Commons Attribution (CC BY) license (https://creativecommons.org/licenses/by/4.0/).

1. Introduction

Long-term and intense tectonic activity has shaped the complex topography and landforms along the eastern margin of the Tibetan Plateau, providing the material foundation and external conditions conducive to landslide formation. The erosion and deposition processes within the region's water systems are key drivers of landscape evolution and geological hazards [1]. The Daduhe river, a major river system on the eastern edge of the Qinghai-Tibet Plateau, has recorded regional tectonic activity since the Late Cenozoic and serves as a crucial site for studying landscape evolution and surface uplift. Large landslides along the Daduhe river basin have significantly influenced the river's evolution [2].

Landslides are gravity-driven surface processes that play a crucial role in regulating landscape evolution in mountainous regions. On one hand, landslides represent an adjust-

ment of slope materials. In areas with intense tectonic activity, rock uplift and river erosion increase the slope gradient, leading to a gradual decline in slope stability. Consequently, landslides are common occurrences along riverbanks. On the other hand, landslides alter the terrain, influencing the subsequent evolution of the landscape. For example, a large landslide that forms a dam in a river channel can trigger the accumulation of extensive and persistent deposits upstream, significantly affecting the river's longitudinal morphology [2]. Thus, the undulating terrain of a region results not only from the long-term interaction between structural forces and surface erosion but also from the ongoing migration and redistribution of materials [2–9].

Landslides represent a disruption of equilibrium conditions, with slope stability primarily determined by topographic features and the properties of slope materials. Key geomorphic indicators, such as elevation, slope gradient, aspect, curvature, lithology, and distance to fault zones and rivers, have long been essential in studies of landslide spatial distribution, providing a foundation for understanding landslide-prone environments [10–17]. However, traditional geomorphic indicators mainly describe the static characteristics of slopes. From the perspective of geomorphic evolution, tectonic activity, landform evolution stages, and material migration processes play a crucial role in the spatiotemporal coupling mechanisms of landslides. In recent years, geomorphic indices, particularly those related to tectonic geomorphology, have become essential tools for studying mountain landscape evolution, river erosion, and tectonic activity [18]. According to Davis's geomorphic erosion cycle theory, catchment development progresses through distinct stages: youth, maturity, and monadnock [19]. Based on this concept, Strahler [20] introduced the hypsometric integral (*HI*) curve to quantify landscape evolution stages [20,21]. The *HI* value represents the residual volume of a catchment following erosion and has been widely applied in geomorphology, hydrology, and active tectonics research [22–25]. Previous studies have demonstrated that the *HI* value not only reflects a catchment's erosion history and tectonic activity [26] but also serves as an indicator of geological hazard development. For example, Lifton et al. [23] identified a positive correlation between *HI* values and crustal uplift rates, while Masek et al. [27] observed that variations in hypsometric curves reflect differences in erosion rates. Duan et al. [28] established a method for predicting mountain hazard risks based on catchment evolution stages, whereas Zhao et al. [29] applied *HI* values to quantitatively classify the debris flow development stages in the Bailongjiang river basin, providing theoretical support for geological hazard prevention. Similarly, Zhang et al. [30] classified the geomorphic evolution stages of 147 debris flow sub-catchments in the upper Minjiang river, revealing that debris flow outbreaks in this region predominantly occur during the mature and early mature stages. Thus, the *HI* value not only reflects landscape evolution stages and the intensity of tectonic activity but also serves as a critical indicator for assessing the spatial distribution of geological hazards. It plays a significant role in understanding the mechanisms driving landslides and related disasters.

In addition to serving as an indicator of landscape evolution and geological hazards, the *HI* value is also closely linked to fluvial processes. Landslides and river dynamics are inherently interconnected: while landslides contribute to sediment flux and alter channel morphology, river incision and lateral erosion can destabilize hillslopes, triggering further mass movements. Large landslides can significantly influence river long profiles by introducing knickpoint steepened segments in the channel that affect sediment transport and incision rates, thereby modifying landscape evolution over timescales of up to 10^4 years [31]. The river steepness index (k_{sn}) is a key parameter for characterizing river longitudinal profile morphology, primarily influenced by factors such as lithology, erosion resistance, and tectonic uplift rates [32,33]. Studies have shown that regions experiencing higher uplift rates generally exhibit increased k_{sn} values [34,35], which in turn correlate with

the occurrence of landslides by affecting slope stability and sediment transport dynamics. Similar correlations have been observed in various tectonically active regions, such as the Northern Tianshan, Helan Mountain Piedmont, Northern Qilian Mountains, and Northern Altun Fault [22,36,37]. These findings reinforce the notion that landslides are integral to landscape evolution, playing a crucial role in balancing tectonic uplift and river incision over extended timescales.

Due to its tectonic and landform characteristics, along with numerous large ancient landslide events, the Daduhe river basin serves as an ideal location for studying the influence of landscape evolution on the spatial distribution of landslides. This study examines the spatial distribution of large landslides in the primary river channel catchments of the Daduhe river. By analyzing the hypsometric integral (*HI*) distribution of the catchments along the river, the study explores how landform features influence the evolution of the Daduhe river and the occurrence of large landslides. The findings aim to provide a scientific basis at the regional landform level for understanding landslide dynamics.

2. Study Area

The Daduhe river, situated along the eastern edge of the Tibetan Plateau to the west of the Sichuan Basin (Figure 1a) is a major tributary of the Yangtze River, originating from the southern slopes of the Guoluo Mountains in Qinghai Province. The river initially flows southwest through regions such as Jinchuan county, Danba county, and Luding county. At Shimian county, it shifts eastward, forming an 'L'-shaped course before merging with the Minjiang river at Xiaogongzui in Leshan City. The Daduhe river stretches approximately 1050 km in length, with a basin area of 77,700 km^2.

The Daduhe river basin is characterized by high, steep mountains interspersed with extensive gullies and ravines. The river traverses this rugged terrain, creating a distinct landscape pattern: high elevations in the northeast and lower elevations in the southwest, with the right bank generally higher than the left. The topography exhibits considerable elevation differences, with Gongga Mountain, the highest point in the basin, reaching approximately 7500 m, while the lowest point at the river's mouth is around 500 m. Notably, Gongga Mountain is located less than 30 km from the river, and the dramatic 6500 m drop in elevation results in intensified river erosion and incision, forming a canyon more than 2000 m deep. The steep slopes and deep valleys create an environment prone to slope failures, significantly influencing the spatial distribution of landslides and the basin's overall geomorphic evolution, as reflected in the hypsometric integral values.

The eastern margin of the Tibetan Plateau, where the Daduhe river basin is situated, has accumulated significant strain energy due to the ongoing uplift and compression of the plateau. This tectonic activity has altered the regional stress distribution [38] and facilitated the formation of several large-scale strike-slip and retroflection fault zones [39]. The Xianshuihe fault zone, located near the Daduhe river basin, has historically exhibited strong seismic activity. Since seismic records began in 1725, 22 earthquakes with magnitudes above Ms6.0 have occurred along this fault zone, including eight earthquakes with magnitudes exceeding Ms7.0. These seismic events play a critical role in triggering large landslides, reshaping the landscape, and modifying river profiles. The interaction between tectonic activity and the region's steep topography directly influences the development of landslides and other mass-wasting processes (Figure 1b).

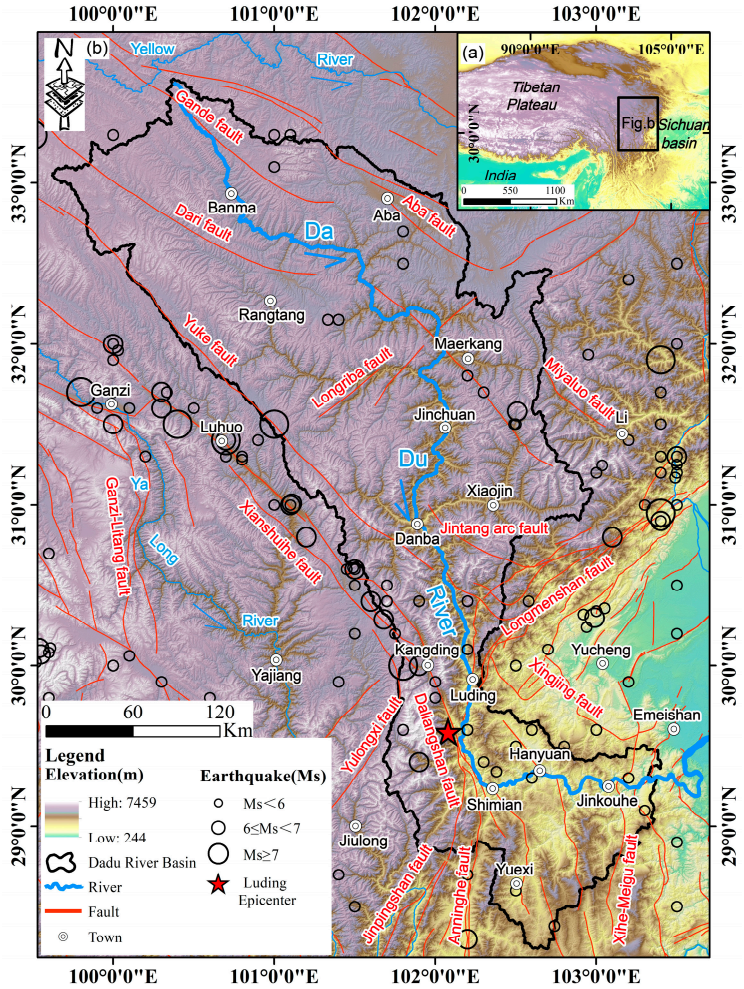

Figure 1. (**a**) Location of Daduhe river basin; (**b**) Tectonic setting of Daduhe river basin.

The Daduhe river basin is a high-risk area for geological disasters in China, and the complex tectonic activities and topography of the region create a favorable environment for the development of earthquake-related geological disasters. Of the nearly 2000 geological disasters recorded in the Daduhe river basin, 801 were landslides and 756 were mudslides. Many of these events blocked the river channels and formed natural dams or weirs [40], severely affecting local ecosystems and livelihoods.

3. Data and Method

3.1. DEM and Remote Sensing Image Data

The DEM data used in this study were sourced from the ASTER GDEM V3 digital elevation products, which have a resolution of 30 m. These products were developed jointly by Japan's METI and NASA (https://search.earthdata.nasa.gov) and have been validated by previous studies, which reported their vertical and horizontal accuracy [41,42]. Slope data were then derived using the ArcGIS 10.8 platform for further analysis.

The remote sensing images for this study were obtained from the Google Earth platform. Compared to other remote sensing data, Google Earth images offer higher resolution and broader coverage. The platform allows for the selection of imagery from different years, facilitating comparative analysis and yielding more accurate landslide identification results in the study area.

3.2. Visual Interpretation Signs and Identification Methods of Large Ancient Landslides

The study area, characterized by vast and rugged mountainous terrain, features a wide distribution of landslides. For the landslide data collection method, we conducted a visual interpretation of remote sensing images. Using Google Earth, the distribution of landslides was observed in detail in high-resolution remote sensing images and their corresponding 3D views, and the landslide boundaries were manually mapped based on markers such as color, texture, and topographic information provided by the images [10]. This process ensured that the landslide boundaries were accurately outlined and provided a reliable data base for subsequent landslide analyses.

Landslides in the study area exhibited distinctive features in the images, including dustpan or tongue-shaped formations, as well as other irregular shapes that sharply contrasted with the surrounding terrain (Figure 2a–d). In some cases, large landslides gave rise to landforms such as platforms or secondary landslides. Large landslides produce landforms such as terraces or secondary landslides. In terms of color, the landslide masses often appeared darker due to vegetation cover and soil erosion. The texture of these areas was characterized by loose deposits, which were easily eroded by flowing water, forming gullies that reflect the historical evolution of landslides. Some large-scale ancient landslides have evolved into important areas for human habitation and farming, reflecting the historical evolution of landslides. Additionally, indirect indicators such as changes in landforms and the water system further contributed to landslide identification.

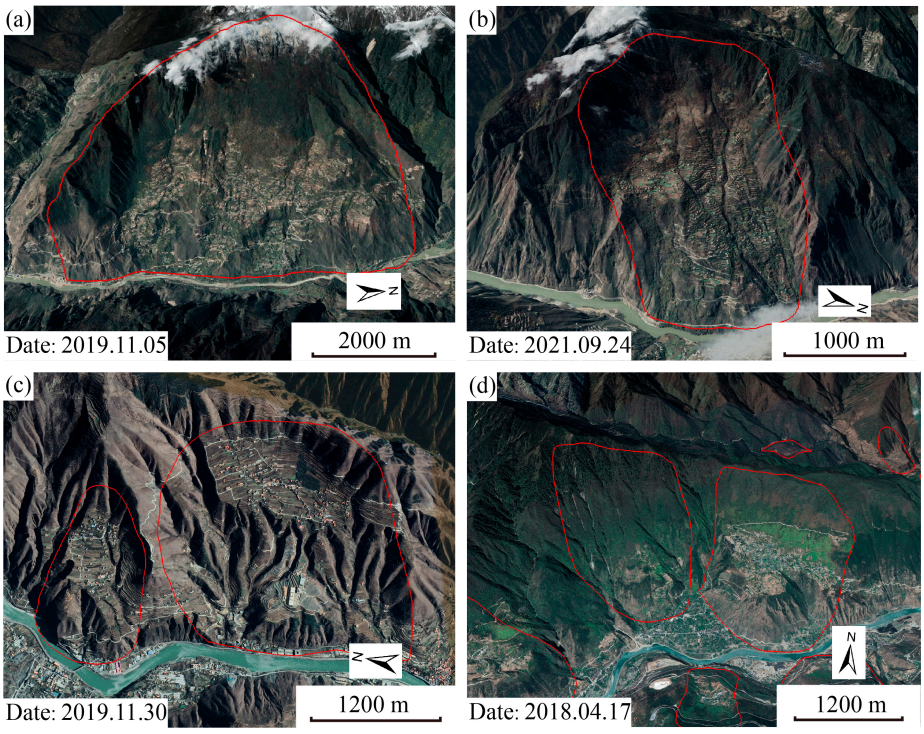

Figure 2. Map showing the satellite images of typical landslide disasters in the Daduhe river basin provided by Google Earth. (**a**) The geographical location is 30.94°N, 101.87°E; (**b**) The geographical location is 30.83°N, 101.90°E; (**c**) The geographical location is 31.50°N, 102.07°E; (**d**) The geographical location is 29.80°N, 102.19°E. (The red circles delineate the outer boundaries of landslides).

Further area calculations and impact factor analysis of landslide data are carried out in ArcGIS 10.8.

3.3. Hypsometric Integral

Strahler [20] provided a quantitative framework for the geomorphic erosion cycle theory proposed by Davis [19] by utilizing the hypsometric integral curve in his study of catchments. This method used the area ratio of the catchment (a/A) as the horizontal coordinate and the elevation ratio (h/H) as the vertical coordinate, plotting a series of points. A polynomial fit to the plotted points generates a curve called the hypsometric curve, and the area under the curve is known as the hypsometric integral (HI).

When the topography of a catchment has undergone long-term evolution and intense erosion, the HI curve exhibits a concave shape with a low HI ($HI \leq 0.4$), corresponding to the monadnock landscape development stage. Conversely, if the topography has experienced short-term evolution and minimal erosion, the HI curve is convex with a high HI ($HI > 0.6$), representing the youth stage of landscape development. The landscape development stage between these extremes is referred to as maturity (Figure 3a) [20].

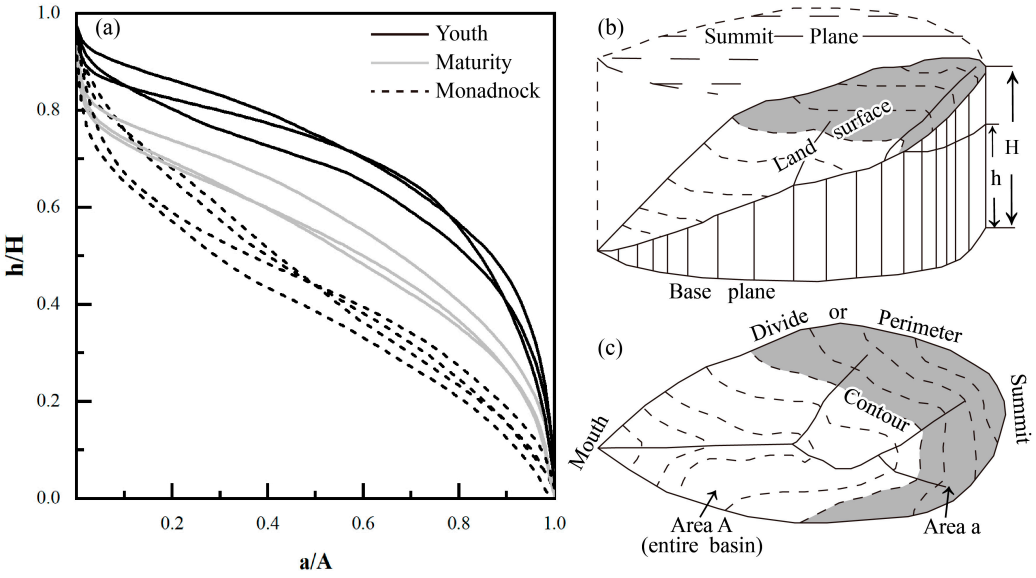

Figure 3. (**a**) Hypsometric curve; (**b**,**c**) Hypsometric integral calculation principle (adapted from Strahler, 1952) [20].

As shown in Figure 3b,c, Area a represents the surface area from a given elevation to the summit of the catchment, while Area A is the total surface area of the catchment. The variable H represents the elevation difference between the highest and lowest points within the catchment, while h denotes the elevation of any given point within the catchment relative to its lowest point. Both H and h can be obtained in ArcGIS 10.8 through simple calculations based on the DEM.

In this study, we employed the method for estimating HI values derived by Pike et al. [43], following the deduction of relevant mathematical formulae. Specifically, the undulation ratio method was used to calculate HI, and it is expressed by the following formula:

$$HI \approx \frac{H_{mean} - H_{min}}{H_{max} - H_{min}}$$

H_{mean}, H_{max}, and H_{min} represent the mean, maximum, and minimum values of elevation for each catchment, respectively. These values were obtained directly using the Zonal Statistics tool in ArcGIS, which subsequently facilitated the calculation of HI values.

4. Results

4.1. Distribution of HI Values in Catchments of Daduhe River's Mainstem

Suhail et al. [38], in their study of the Daduhe river basin catchments, only considered the catchments of tributaries that converge with the river's mainstem. They did not address the areas through which the river mainstem flows, despite the fact that landslides frequently occur along the free surfaces formed by cutting and erosion on both sides of the river. Therefore, to comprehensively analyze the development characteristics of the river's mainstem catchments, this study also includes these areas.

Utilizing the Hydrology toolbox in ArcGIS 10.8, this study identified a total of 601 catchments on both sides of the Daduhe river's mainstem (Figure 4). These catchments were further classified into two categories based on their connectivity to the mainstem. Type I includes the catchments of tributaries that converge with the river's mainstem (represented by the red catchments in Figure 4), totaling 363 catchments. Type II encompasses the catchments through which the river mainstem flows (indicated by the blue catchments in Figure 3), comprising 238 catchments. The number of watershed samples, after the power analysis, would provide a power greater than 80% to detect a medium effect size with d = 0.5 at a significance level of $\alpha = 0.05$ in a two-tailed independent t-test. This indicates that the conclusions of this paper, which are based on these watershed data, are reliable [44].

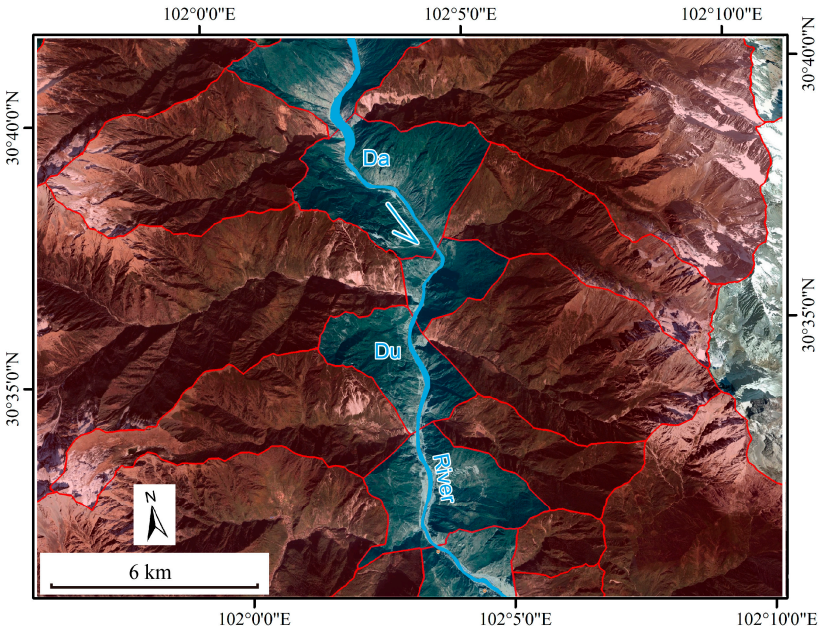

Figure 4. Distribution of Daduhe river's catchments. The red areas are the catchments where tributaries merge into the mainstem (Type I). The blue areas are where major rivers flow through catchments (Type II).

The hypsometric integral (*HI*) reflects the distribution of elevation within a catchment [20,45]. In general, a high *HI* value indicates rapid uplift with relatively little erosion or a later stage of landform development that retains more lithological features. Conversely, a low *HI* value suggests that the surface has experienced significant erosion and is largely unaffected by surface deformation at the present stage [38].

While lithology and tectonic uplift can influence *HI* values at a local scale [24], the threshold values proposed by Strahler [20] provide a widely accepted framework for assessing relative landscape maturity. The *HI* values of the Daduhe river's mainstem catchments ranged from 0.35 to 0.71 and were categorized into three groups: youth ($HI \leq 0.4$), maturity ($0.4 < HI \leq 0.6$), and monadnock ($HI > 0.6$) [20]. Of these, 79 youth catchments were

located in the Banma–Danba section, and 331 maturity catchments were distributed in the Danba–Shimian section. The 191 monadnock catchments were situated in relatively gentle terrain, mainly in areas such as the upper reaches of Banma County and the lower reaches of Shimian–Jinkouhe County (Figure 5). Most catchments fall under the category of maturity, indicating active surface erosion.

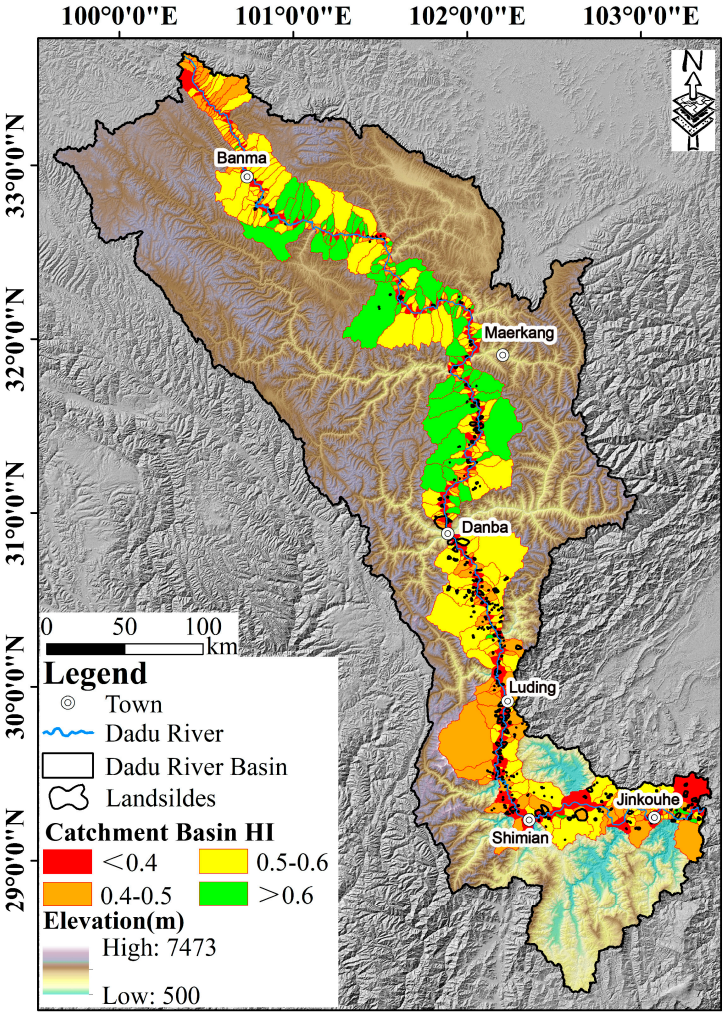

Figure 5. Distribution of landslides and *HI* values of catchments in Daduhe river basin.

4.2. Distribution of Large Landslides in the Catchments of Daduhe River's Mainstem

Based on the Google Earth platform, a total of 477 large landslides were identified in the catchments on both sides of the river's mainstem. The largest landslide covered an area of 42.31 km^2, while the smallest measured 0.002 km^2, with an average landslide area of 0.78 km^2. The spatial distribution of these landslides is shown in Figure 6.

The probability density analysis yielded a curve that predominantly follows a monotonically decreasing pattern (Figure 7), which is commonly associated with the power-law recurrence relationships observed in landslide distributions [46]. Although the results show a K-S test statistic of D = 0.0794 and p = 0.0056, indicating that the landslide area data deviate from a lognormal distribution at the 95% confidence level, previous studies have demonstrated that landslide area distributions can vary due to regional differences, geological settings, data completeness, and classification criteria [47,48].

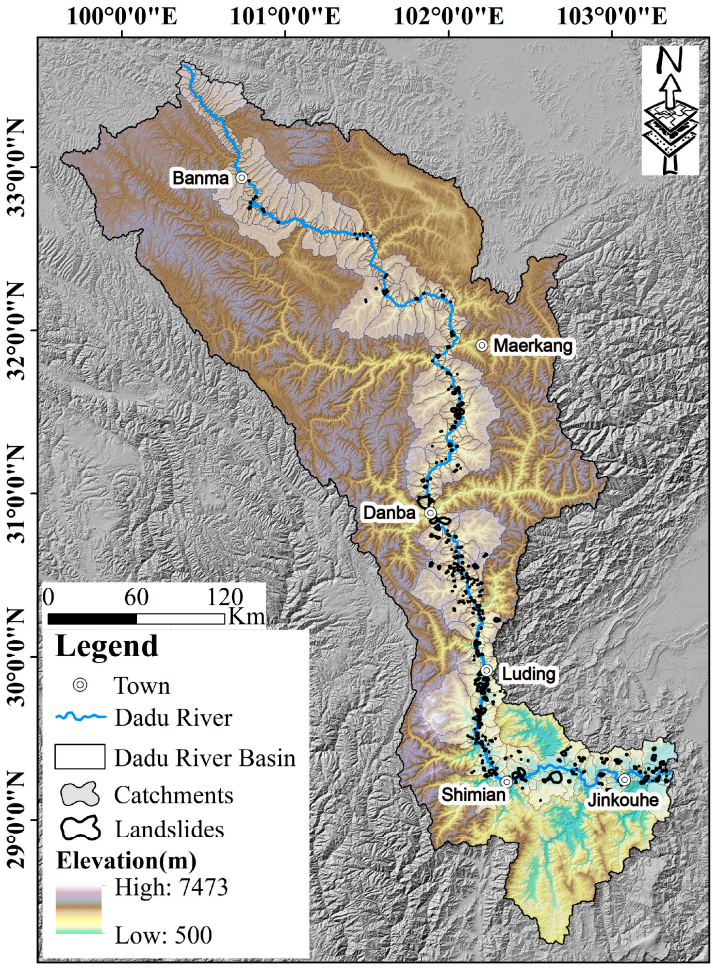

Figure 6. Large landslides' distribution in the catchments of Daduhe river's mainstem.

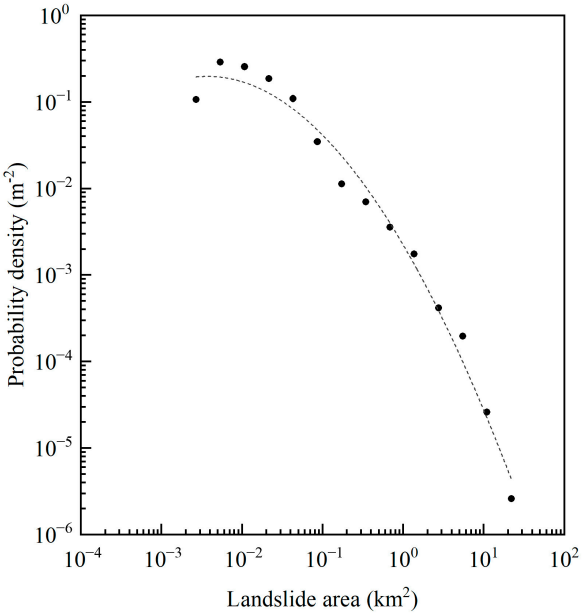

Figure 7. Probability density distribution of large landslides in catchments of Daduhe river's mainstem.

In this study, the landslide dataset primarily comprises large-scale ancient landslides within the catchment area of the Daduhe river's mainstem. These landslides have under-

gone prolonged weathering, which may obscure their boundaries and introduce some uncertainty in landslide area measurements. However, our primary analysis does not rely on landslide areas strictly adhering to a specific probabilistic model, but rather focuses on the spatial distribution characteristics of landslides and their relationship with geomorphological parameters. Therefore, despite the deviation from a lognormal distribution, our dataset remains robust and suitable for analyzing landslide distribution patterns.

As shown in Figure 6, the distribution of large landslides in the Daduhe river basin is uneven. Fewer landslides are observed in the section from the river's source to Maerkang county, while the landslide distribution is more concentrated between Maerkang county and Danba county. The most intensive landslide activity occurs between Danba county and the downstream outlet, particularly near Luding county. The largest landslide, the Ganhaizi landslide upstream of Danba county, has a volume that qualifies it as a "huge" landslide.

The landscape features of the large landslides are clearly visible in the remote sensing image maps (Figure 2a–d). These landslides are large in scale, exhibiting various shapes, such as tongues and semicircles, with well-defined boundaries and prominent trailing edges. Additionally, the loss of rock and soil mass from the landslides has caused noticeable sagging of the terrain compared to the surrounding landscape. Deposition frequently occurs at the slope foot near the riverbank, altering the natural flow of the river and causing the river to curve toward the opposite bank. The landslide areas are characterized by sparse vegetation, exposed soil and rock, and clear signs of collapse, making them easily identifiable in the images.

The elevation of the Daduhe river basin ranges from 500 m to 7473 m, with the terrain generally sloping from higher elevations in the northwest to lower elevations in the southeast. The river itself flows at relatively low elevations. The average slope of the basin is approximately 24°, with particularly steep slopes on both sides of the river, exhibiting typical fluvial landform characteristics. This study statistically analyzes the distribution of landslides at different elevations and slopes along the river's mainstem using two evaluation indices: the landslide number density (LND) and landslide area percentage (LAP). The LND represents the number of landslides per km^2, while the LAP indicates the percentage of the total landslide area within each classified category [10–12]. The calculation formula for the LND and LAP is as follows:

$$LND = \frac{The\ number\ of\ landslides\ in\ each\ classification}{The\ area\ of\ each\ classification}$$

$$LAP = \frac{The\ area\ of\ landslides\ in\ each\ classification}{The\ area\ of\ each\ classification} \times 100\%$$

In regions with substantial elevation differences, pronounced topographical variations reduce soil resistance to gravitational forces, thereby accelerating water flow and increasing soil erosion and dissolution. These processes, in turn, enhance the likelihood of landslides [49]. The elevation of the river's mainstem catchments was divided into six classifications, each spanning 1000 m (Figure 8a): (1) <1000 m; (2) 1000~2000 m; (3) 2000~3000 m; (4) 3000~4000 m; (5) 4000~5000 m; and (6) >5000 m. The statistical results are shown in Figure 9a. Both the landslide number density (LND) and landslide area percentage (LAP) increase with elevation, peaking in the 1000~2000 m range, before decreasing at higher elevations. No landslides were observed above 5000 m.

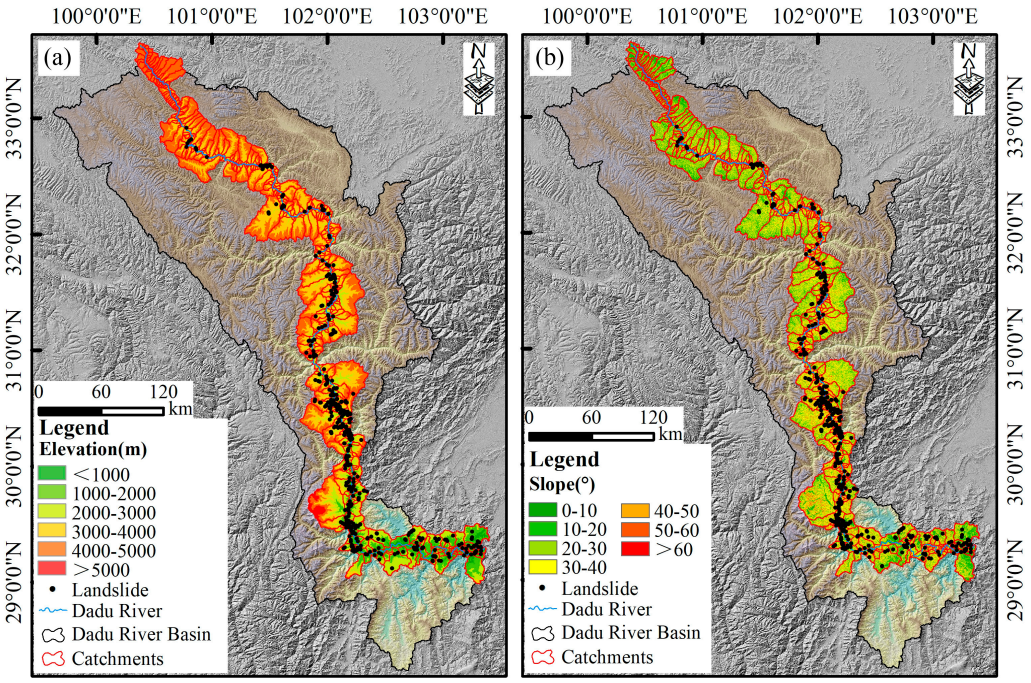

Figure 8. Elevation and slope distribution in catchments of Daduhe river's mainstem. (**a**) Elevation; (**b**) Slope.

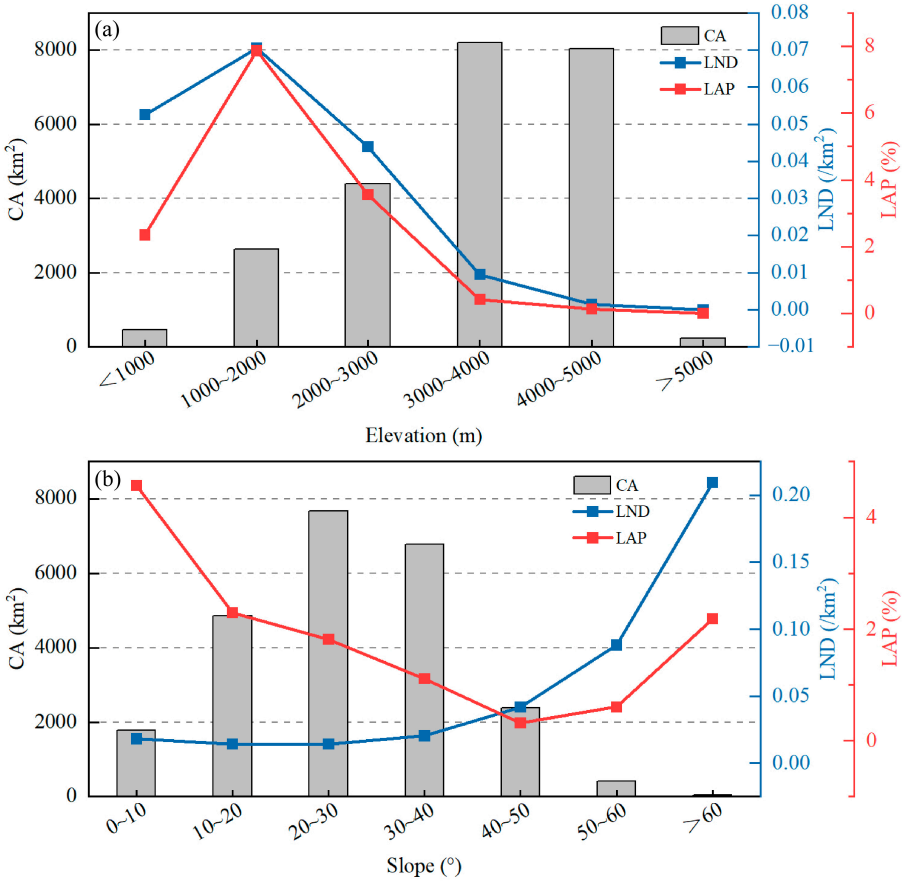

Figure 9. The relationship between landform factor, LND, and LAP of large landslides. (**a**) Elevation; (**b**) Slope. (CA is the area of the study area corresponding to each classification; LND is landslide number density; LAP is landslide area percentage).

Slope refers the degree of ground inclination and is a crucial factor in the occurrence of landslides. It primarily influences slope stability by determining the magnitude and direction of stress within the slope body, thereby affecting surface runoff and material movement [50]. The slope of the catchments was classified into seven categories with 10° intervals (Figure 8b): (1) 0~10°; (2) 10~20°; (3) 20~30°; (4) 30~40°; (5) 40~50°; (6) 50~60°; and (7) >60°. The statistical results are shown in Figure 9b. The landslide number density (LND) exhibits an exponential growth trend with increasing slope, indicating that steeper slopes are more prone to landslides. However, the landslide area percentage (LAP) initially decreases and then increases as the slope steepness increases, peaking in the 0–10° range. This may be due to the fact that landslide accumulations in remotely sensed images are predominantly found on flatter slopes, which causes some landslides to appear in less steep areas. Conversely, landslides on steeper slopes are less likely to remain intact and may not be detected, resulting in a lower number of landslides in these areas. Large landslides have a significant impact on the surrounding terrain. The occurrence of large landslides can transform previously steep terrain into gentler, more stable slopes. This helps explain why the LND is low but the LAP is high in the 0–10° range, reflecting the role of landslides in terrain modification. In contrast, in areas with slopes exceeding 60°, both the LND and LAP are high, indicating the strong influence of slope steepness on the occurrence of landslides.

4.3. Relationship Between Catchment Type, HI Values, and Large Landslide Distribution

An analysis of the large landslide distribution in the two types of catchments (Figure 10a) reveals distinct differences between them. Specifically, both LND values and LAP values are higher in Type II catchments compared to Type I catchments. Additionally, the average *HI* value is greater for Type I catchments than for Type II catchments. These findings indicate that large landslides are more likely to occur in Type II catchments. This increased susceptibility may be attributed to the presence of the Daduhe river's mainstem, which runs through these catchments, enhancing surface erosion. The slopes on both sides of the river are particularly affected by the dynamic flow of water, which contributes to slope instability and results in the occurrence of numerous landslides.

In the study area, the landslide distribution is most intense in the Danba–Shimian county section, which corresponds to the maturity stage of landscape development. In this region, strong surface uplift and river erosion create steep riverbank slopes, providing favorable conditions for the occurrence of landslides. The frequent landslides result in the displacement of large amounts of unstable rock and soil, which are then transported by flowing water, leading to a decrease in the *HI* values of catchments. This reduction in *HI* values reflects a key surface erosion process in the transition from youth to monadnock in landform development.

Additionally, the *HI* values in this study were classified into four categories with an interval of 0.1: (1) <0.4, (2) 0.4~0.5, (3) 0.5~0.6, and (4) >0.6. As shown in Figure 10b, both the landslide number density (LND) and landslide area percentage (LAP) decrease as the *HI* values increase. This pattern indicates that catchments in the youth stage of landscape evolution exhibit fewer landslides, while catchments in the monadnock stage tend to have a more widespread landslide distribution.

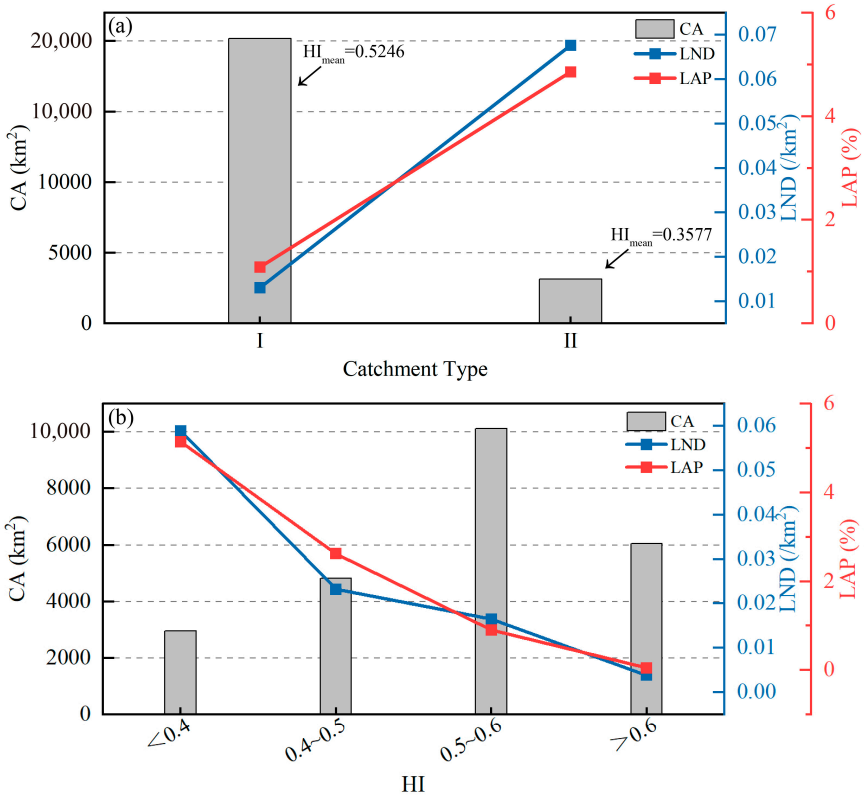

Figure 10. (**a**) The relationship between slope, LND, and LAP of landslides (types I and II are shown in Figure 4; CA is the area of the study area corresponding to each classification); (**b**) The relationship between *HI* values of catchments, LND, and LAP of large landslides.

5. Discussion

5.1. Intrinsic Link Between River Longitudinal Profile Morphology and Landslide Distribution

The normalized steepness index (k_{sn}) is commonly used to analyze the spatial distribution of regional tectonic uplift rates [33,35]. The formula for its calculation is as follows:

$$S = k_{sn} A^{-\theta_{ref}}$$

In the formula, k_{sn} is the normalized steepness index and θ is the concavity index (also known as the curvature) of the longitudinal profile of the river, which indicates the degree of concavity of the longitudinal profile of the river channel in its natural state. Referring to the results of the previous studies, k_{sn} was determined using the reference concavity (θ_{ref} = 0.45) [51,52]. With the determination of the slope (S) and catchment area (A), the steepness index can be calculated for a specific point in the river channel.

In addition, the river knickpoint, which marks the transition between the gently sloping and steep sections of a riverbed, results from geological processes such as backwater erosion and tectonic uplift. The continuous migration of the knickpoint, along with the erosion and downcutting in the region where it forms, serves as an important indicator of landscape evolution within a catchment [51]. Both the k_{sn} and knickpoints serve as important landform parameters that significantly influence the spatial distribution of landslides.

The distribution of k_{sn} values and knickpoints along the Daduhe river's mainstem is shown in Figure 11. In the study area, k_{sn} values ranged from 0 to 2339.13 m$^{0.9}$, with an average value of 164.70 m$^{0.9}$. Overall, the k_{sn} values exhibited a decreasing trend from south to north, with notably higher values in Danba county–Luding county (the red polyline), where the average k_{sn} reached 301.43 m$^{0.9}$. A total of 27 knickpoints were identified along

the river's mainstem, with the highest concentration occurring between Danba county and Shimian county. Notably, the k_{sn} values were consistently higher downstream of these knickpoints (the orange dotted line in Figure 11). Landslides near these knickpoints tended to have significantly larger volumes, especially in the areas around Danba county and Shimian county. These landslides served as major sediment sources, with a large number flowing into the river channel, forming natural dams that obstructed the river's flow. These obstructions altered the local slope of the river's longitudinal profile, leading to elevated k_{sn} values and creating favorable conditions for knickpoint formation [2].

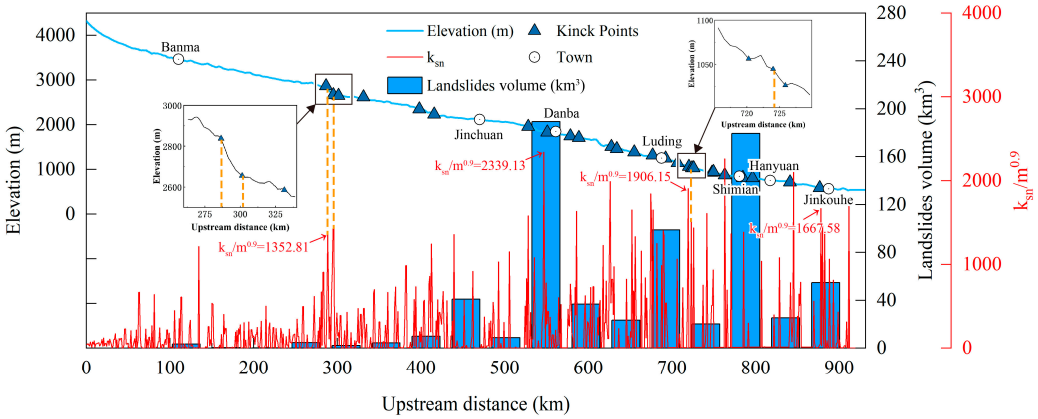

Figure 11. Correlation analysis between longitudinal profile of Daduhe river's mainstem and landslide volume of catchment, k_{sn}, and knickpoints.

At the same time, variations in regional crustal uplift rates contributed to the local increase in k_{sn} values and the development of knickpoints. This alters the river's erosion base, enhances both downward and lateral erosion, steepens riverbank slopes, and promotes the initiation and development of landslides. In turn, landslides along the riverbanks and their subsequent accumulation within the channel contribute to the formation of new knickpoints. This intricate interaction between tectonic activity and landslide dynamics drives the evolution of mountainous landscapes and the dynamic development of river systems. Ultimately, landslide-induced geomorphic changes play a pivotal role in landscape evolution. The influence of landslides on knickpoint formation, channel morphology, and the long-term redistribution of sediments warrants further investigation.

5.2. The Relationship Between Uneven Distribution of Large Landslides and Landscape Evolution

Large landslides in the study area exhibit an uneven, segmental distribution along the river, with a corresponding segmental distribution in the *HI* values of the river's mainstem catchments. A clear relationship can be observed between these two patterns: in the Banma–Danba section, the catchments are in a transitional stage from youth to maturity ($HI > 0.5$), where landslides are less frequent. In contrast, the catchments from Danba to the downstream outlet are transitioning from maturity to monadnock ($HI < 0.5$), exhibiting a more concentrated distribution of landslides. The statistical results shown in Figure 10b further confirm that lower *HI* values correspond to a higher density of landslides within catchments, highlighting the significant influence of landscape development stages on the landslide distribution. In other words, as the catchments progress from youth to monadnock, factors such as elevation, slope, and terrain undulation evolve, controlling the development of landslides. Consequently, the frequency and density of landslides serve as indicators of the landscape evolution process.

Landslides are not merely passive responses to landform characteristics; they also play a critical role in shaping landscape evolution. When a landslide occurs, large volumes of

rock and soil rapidly slide down the slope, altering the local topography and influencing the broader geomorphic pattern through material accumulation and transport. This creates a dynamic feedback loop between landslide activity and landscape evolution: while the occurrence of landslides is influenced by existing landform features, it simultaneously drives the continuous transformation of the landscape.

Due to the large scale and complex topography of landslides in the study area, the actual measurement of landslide volume is difficult to achieve. Although the estimated volume may not perfectly represent the actual landslide volume, it provides a reasonable approximation for our analysis. Therefore, the empirical area–volume formula proposed by Larsen et al. [7] based on 4231 landslide data around the world was used in this study to estimate the landslide volume. This formula has been validated in other regions and is widely recognized for its applicability, making it sufficient for our research needs [16].

$$V = 0.146 * A^{1.335}$$

In the formula, V is the estimated landslide volume and A is the landslide area. In order to more accurately represent the role of landslides in controlling the evolution of topography and landscape, this study proposes a simple landslide volume recovery method.

Assuming all landslide material has been removed (Figure 12a), the denudation volume was estimated by the empirical landslide area–volume formula, and the average thickness of the landslide was superimposed back to its original position (Figure 12b), thus providing an approximate estimate of the landslide volume as a proportion of the pre-denudation volume of each catchment (Figure 12c), which was verified with an *HI* curve. This method was designed to assess the specific effects of landslide activity on landscape evolution within catchments, and the calculations are based on the following formulae:

$$\text{Landslide volume ratio} = \frac{\sum_{i=1}^{n} 0.146 * A_i^{1.335}}{(H_{max} - H_{min}) * A_C} \times 100\%$$

where A_i is the landslide area, n is the number of landslides in each catchment, H_{max} is the maximum catchment elevation, H_{min} is the minimum catchment elevation, and A_C is the catchment area.

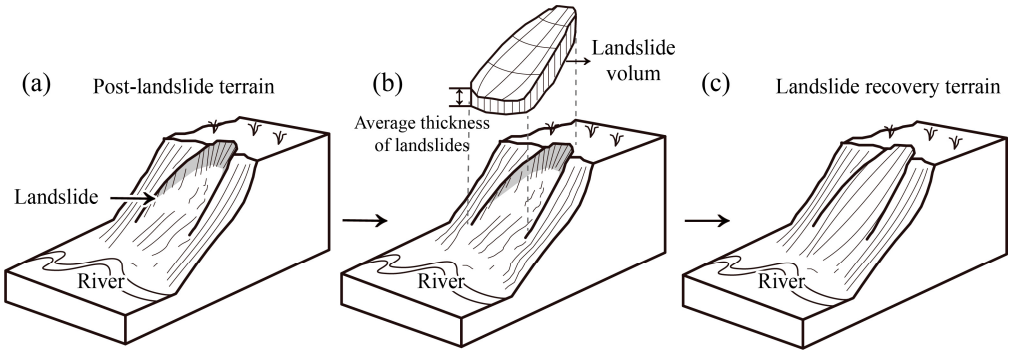

Figure 12. Landslide volume recovery method.

The analysis results presented in Figure 13 show a progressive increase in the modification of catchment geomorphology by landslides from north to south along the river. Specifically, the proportion of landslide volume to the total pre-denudation volume of the catchments can reach up to 105.7%, with an average of 2.68%.

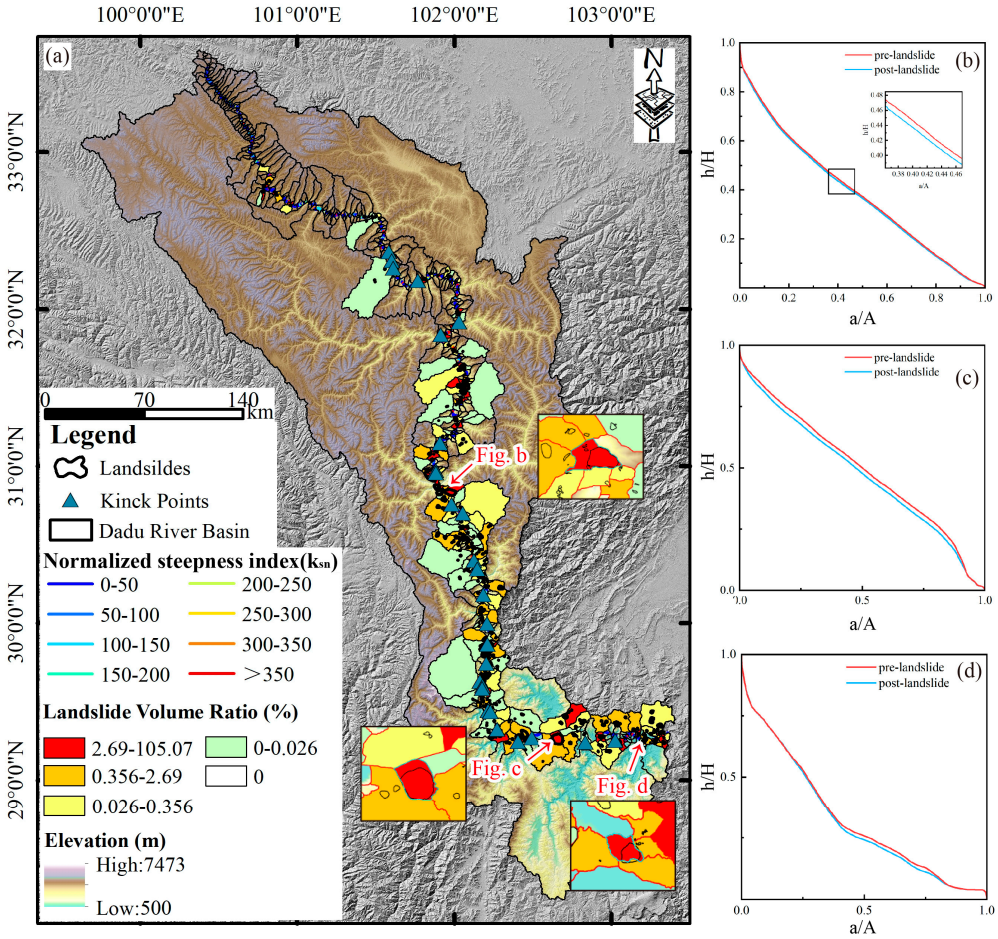

Figure 13. (**a**) Influence of landslide development on the amount of denudation in catchments. (**b**–**d**) Changes in *HI* curves in catchments before and after landslides.

The "Landslide Volume Ratio" in Figure 13a exceeds 100%, primarily due to two factors. First, uncertainties in the pre-erosion volume estimation can lead to an underestimation of the total sediment storage and an inflated volume ratio. Since reconstructing pre-erosion topography relies on assumptions, the highest pre-erosion elevation (original highest elevation) often exceeds the highest elevation used in our calculations (current highest elevation), indicating that the watershed's highest points have undergone weathering and erosion. Second, the potential overestimation of landslide volume may contribute to this phenomenon, as the volume–area scaling relationship proposed by Larsen et al., while widely applicable, does not account for local variations in landslide geometry, material properties, and failure mechanisms, which may lead to an overestimation of landslide volumes in specific cases.

These results demonstrate that the development of large landslides has had a profound impact on the landscape evolution of the catchments. The *HI* curve of the catchments becomes concave after landslides, indicating that landslides have significantly contributed to the landscape evolution in a short period. This highlights the crucial role of landslides as a key surface process in the landscape evolution of the catchments. These findings not only deepen our understanding of the interaction between landslides and geomorphology in catchments but also provide valuable insights for geological disaster prevention and the development of landscape evolution models in catchments.

6. Conclusions

In this study, we thoroughly analyzed the distribution patterns of *HI* values within the catchments along the Daduhe river's mainstem. By examining the variations in *HI* values, we explored their relationship with the landslide distribution and landscape evolution. Our findings suggest that landscape evolution indicators can provide valuable insights for identifying landslide-prone regions, contributing to a better understanding of landslide susceptibility. The main conclusions are as follows:

(1) The *HI* values within the catchments of the Daduhe river's mainstem ranged from 0.35 to 0.71, showing a phased progression from youth to maturity and monadnock stages from upstream to downstream. The Banma–Danba section corresponds to the youth stage, the Danba–Shimian section corresponds to the maturity stage, and the regions between Shimian and Jinkouhe are characteristic of the monadnock stage of fluvial landscape evolution. This progression suggests an overall transition from an active incision in the upper reaches to a more stabilized landscape in the lower reaches;

(2) In catchments along the Daduhe river's mainstem, 477 large landslides were identified, which exhibit a clear spatial correlation with the *HI* values. Landslides were less frequent in the Banma county–Danba county area ($HI > 0.5$), while a higher density was observed in the section from Danba county to the river outlet ($HI < 0.5$). Most large landslides occurred in areas with elevations between 1000 and 2000 m, slopes < 40°, *HI* values < 0.4, higher k_{sn} values, and a dense distribution of knickpoints. These findings indicate that catchments in the maturity to monadnock stages are more susceptible to large landslides, likely due to the combined effects of river incisions and structural weakening;

(3) Large landslides significantly influence river morphology by obstructing the river's flow and promoting knickpoint formation. Their influence on catchment landscapes increases progressively from north to south, aligning with the observed transition in landscape evolution stages. On average, landslide volume constitutes 2.68% of the total pre-denudation volume of catchments. Following the occurrence of large landslides, the *HI* curves of the catchments become concave, highlighting the critical role of landslides in driving rapid landscape evolution.

Our study highlights the spatial relationship between landscape evolution indicators (e.g., *HI* and k_{sn}) and the occurrence of landslides, offering valuable insights for landslide hazard assessment. These geomorphic parameters could serve as effective proxies for identifying landslide-prone areas, enhancing regional susceptibility models. Integrating our spatial database with landscape evolution models, along with leveraging emerging InSAR time-series data, could provide a more dynamic understanding of post-landslide channel adjustments.

Author Contributions: Conceptualization, X.C.; Methodology, M.B.; Formal analysis, M.B.; Resources, H.Q.; Data curation, H.Q.; Writing—original draft, M.B.; Writing—review & editing, X.C.; Funding acquisition, X.C. All authors have read and agreed to the published version of the manuscript.

Funding: This research was funded by [Institute of Geology, China Earthquake Administration] grant number [IGCEA2202].

Data Availability Statement: The original contributions presented in this study are included in the article. Further inquiries can be directed to the corresponding author.

Acknowledgments: This research was supported by the National Nonprofit Fundamental Research Grant of China, Institute of Geology, China Earthquake Administration (grant no. IGCEA2202).

Conflicts of Interest: The authors declare no conflicts of interest.

References

1. Harkins, N.; Kirby, E.; Heimsath, A.; Robinson, R.; Reiser, U. Transient fluvial incision in the headwaters of the Yellow River, northeastern Tibet, China. *J. Geophys. Res.* **2007**, *112*. [CrossRef]
2. Ouimet, W.B.; Whipple, K.X.; Royden, L.H.; Sun, Z.; Chen, Z. The influence of large landslides on river incision in a transient landscape: Eastern margin of the Tibetan Plateau (Sichuan, China). *Geol. Soc. Am. Bull.* **2007**, *119*, 1462–1476. [CrossRef]
3. Burbank, D.; Blythe, A.; Putkonen, J.; Pratt-Sitaula, B.; Gabet, E.; Oskin, M.; Barros, A.; Ojha, T. Decoupling of erosion and precipitation in the Himalayas. *Nature* **2003**, *426*, 652–655. [CrossRef]
4. Densmore, A.L.; Anderson, R.S.; McAdoo, B.G.; Ellis, M.A. Hillslope evolution by bedrock landslides. *Science* **1997**, *275*, 369–372. [CrossRef] [PubMed]
5. Hales, T.; Roering, J.J. Climatic controls on frost cracking and implications for the evolution of bedrock landscapes. *J. Geophys. Res.* **2007**, *112*. [CrossRef]
6. Korup, O.; Montgomery, D.R.; Hewitt, K. Glacier and landslide feedbacks to topographic relief in the Himalayan syntaxes. *Proc. Natl. Acad. Sci. USA* **2010**, *107*, 5317–5322. [CrossRef]
7. Larsen, I.J.; Montgomery, D.R.; Korup, O. Landslide erosion controlled by hillslope material. *Nat. Geosci.* **2010**, *3*, 247–251. [CrossRef]
8. Montgomery, D.R. Slope distributions, threshold hillslopes, and steady-state topography. *Am. J. Sci.* **2001**, *301*, 432–454.
9. Montgomery, D.R.; Brandon, M.T. Topographic controls on erosion rates in tectonically active mountain ranges. *Earth Planet. Sci. Lett.* **2002**, *201*, 481–489. [CrossRef]
10. Tian, Y.; Xu, C.; Xu, X.; Chen, J. Detailed inventory mapping and spatial analyses to landslides induced by the 2013 Ms 6.6 Minxian earthquake of China. *J. Earth Sci.* **2016**, *27*, 1016–1026. [CrossRef]
11. Wang, W.; Ma, S.; Yan, W.; Yuan, R. The Spatial Distribution Characteristics and Possible Influencing Factors of Landslide Disasters in the Zhaotong Area, Yunnan Province of China. *Appl. Sci.* **2024**, *14*, 5093. [CrossRef]
12. Xu, C. A preliminary spatial distribution analysis of landslides triggered by the 2010 Haiti earthquake. In *Proceedings of the Landslide Science for a Safer Geoenvironment: Volume 3: Targeted Landslides*; Springer: Cham, Switzerland, 2014; pp. 183–190.
13. Yueping, Y. Researches on the geo-hazards triggered by Wenchuan earthquake, Sichuan. *J. Eng. Geol.* **2008**, *16*, 433–444.
14. Dai, F.C.; Xu, C.; Yao, X.; Xu, L.; Tu, X.B.; Gong, Q.M. Spatial distribution of landslides triggered by the 2008 Ms 8.0 Wenchuan earthquake, China. *J. Asian Earth Sci.* **2011**, *40*, 883–895.
15. Huang, F.; Ye, Z.; Jiang, S.-H.; Huang, J.; Chang, Z.; Chen, J. Uncertainty study of landslide susceptibility prediction considering the different attribute interval numbers of environmental factors and different data-based models. *Catena* **2021**, *202*, 105250.
16. Zou, Y.; Qi, S.; Guo, S.; Zheng, B.; Zhan, Z.; He, N.; Huang, X.; Hou, X.; Liu, H. Factors controlling the spatial distribution of coseismic landslides triggered by the Mw 6.1 Ludian earthquake in China. *Eng. Geol.* **2022**, *296*, 106477. [CrossRef]
17. Jin, J.-l.; Cui, Y.-l.; Xu, C.; Zheng, J.; Miao, H.-b. Application of logistic regression model for hazard assessment of landslides caused by the 2012 Yiliang Ms 5.7 earthquake in Yunnan Province, China. *J. Mt. Sci.* **2023**, *20*, 657–669. [CrossRef]
18. Makrari, S.; Sharma, G.; Taloor, A.K.; Singh, M.S.; Sarma, K.; Aggarwal, S. Assessment of the geomorphic indices in relation to tectonics along selected sectors of Borpani River Basin, Assam using Cartosat DEM data. *Geosystems Geoenvironment* **2022**, *1*, 100068. [CrossRef]
19. Davis, W.M. The geographical cycle. In *Climatic Geomorphology*; Springer: Berlin/Heidelberg, Germany, 1973; pp. 19–50.
20. Strahler, A.N. Hypsometric (area-altitude) analysis of erosional topography. *Geol. Soc. Am. Bull.* **1952**, *63*, 1117–1142.
21. Schumm, S.A. Evolution of drainage systems and slopes in badlands at Perth Amboy, New Jersey. *Geol. Soc. Am. Bull.* **1956**, *67*, 597–646.
22. Zhou, C.; He, H.-l.; Wei, Z.-y.; Su, P.; Ren, G.-x. The application of geomorphic indexes in small-scale geomorphology: A case study in dushanzi anticline in the northern chinese tian shan foreland. *Seismol. Geol.* **2020**, *42*, 1492–1508.
23. Lifton, N.A.; Chase, C.G. Tectonic, climatic and lithologic influences on landscape fractal dimension and hypsometry: Implications for landscape evolution in the San Gabriel Mountains, California. *Geomorphology* **1992**, *5*, 77–114.
24. Ohmori, H. Changes in the hypsometric curve through mountain building resulting from concurrent tectonics and denudation. *Geomorphology* **1993**, *8*, 263–277.
25. Willgoose, G. A physical explanation for an observed area-slope-elevation relationship for catchments with declining relief. *Water Resour. Res.* **1994**, *30*, 151–159.
26. Chen, Y.-C.; Sung, Q.; Cheng, K.-Y. Along-strike variations of morphotectonic features in the Western Foothills of Taiwan: Tectonic implications based on stream-gradient and hypsometric analysis. *Geomorphology* **2003**, *56*, 109–137.
27. Masek, J.G.; Isacks, B.L.; Gubbels, T.L.; Fielding, E.J. Erosion and tectonics at the margins of continental plateaus. *J. Geophys. Res. Solid Earth* **1994**, *99*, 13941–13956.
28. Duan, S.-S.; Yao, L.-K.; Guo, C.-W. Tendency Evaluation of Collapse-landslide Caused by Earthquake Based on the Erosion Cycle Theory. *J. Hunan Univ. (Nat. Sci.)* **2015**, *42*, 116–123.

29. Yan, Z.; Xingmin, M.; Feng, Q.; Lintong, L.; Fuyun, G. Stage Division of Debris Flow Torrent Based on Geomorphologic Parameter. *J. Catastrophology* **2018**, *33*, 48–52.
30. Jing, Z.; Shujun, T.; Pengli, H. The material supply ability analysis of debris flows based on areahypsometric integral and area-gradient integral. *Chin. J. Geol. Hazard Control* **2021**, *32*, 9–16. [CrossRef]
31. Korup, O.; Densmore, A.L.; Schlunegger, F. The role of landslides in mountain range evolution. *Geomorphology* **2010**, *120*, 77–90.
32. Willett, S.D.; Hovius, N.; Brandon, M.T.; Fisher, D.M. *Tectonics, Climate, and Landscape Evolution*; Geological Society of America: Boulder, CO, USA, 2006; Volume 398.
33. Duvall, S.F.; Delquadri, J.C.; Ward, D.L. A preliminary investigation of the effectiveness of homeschool instructional environments for students with attention-deficit/hyperactivity disorder. *Sch. Psychol. Rev.* **2004**, *33*, 140–158.
34. Kirby, E.; Whipple, K.X. Expression of active tectonics in erosional landscapes. *J. Struct. Geol.* **2012**, *44*, 54–75. [CrossRef]
35. Kirby, E.; Whipple, K.X.; Tang, W.; Chen, Z. Distribution of active rock uplift along the eastern margin of the Tibetan Plateau: Inferences from bedrock channel longitudinal profiles. *J. Geophys. Res.* **2003**, *108*. [CrossRef]
36. Hongzhuang, Z.; Youli, L.; Jingchun, Y.; Supei, S. Geomorphology Characteristic and Tectonic Response of the Northern Tianshan Represented by Hypsometric Integral. *Mt. Res.* **2009**, *27*, 285–292.
37. Xiaoqian, S.; Jianzhang, P.; Yizhou, W.; Dewen, Z.; Huiping, Z.; Yuqi, H. Late miocene uplift history of the northern qilian shan constrained by the longitudinal profile. *Quat. Sci.* **2024**, *44*, 338–353.
38. Suhail, H.A.; Yang, R.; Chen, H.; Rao, G. The impact of river capture on the landscape development of the Dadu River drainage basin, eastern Tibetan plateau. *J. Asian Earth Sci.* **2020**, *198*, 104377. [CrossRef]
39. Xu, X.; Gao, R.; Guo, X.; Li, W.; Li, H.; Wang, H.; Huang, X.; Lu, Z. Outlining tectonic inheritance and construction of the Min Shan region, eastern Tibet, using crustal geometry. *Sci. Rep.* **2017**, *7*, 13798. [CrossRef]
40. Renji, B.; Li, W.; Wanmo, Z.; Zongliang, L.; Minhui, L.; Yujie, L.; Huayong, N.; Ruge, X. Characteristics and distribution of the geology disasters of the Dadu River in Sichuan, China. *J. Chengdu Univ. Technol. (Sci. Technol. Ed.)* **2011**, *38*, 529–537.
41. Tachikawa, T.; Kaku, M.; Iwasaki, A.; Gesch, D.B.; Oimoen, M.J.; Zhang, Z.; Danielson, J.J.; Krieger, T.; Curtis, B.; Haase, J. ASTER Global Digital Elevation Model Version 2-Summary of Validation Results. USGS Report. 2011, p. 37. Available online: https://ui.adsabs.harvard.edu/abs/2011usgs.rept...37T/abstract (accessed on 9 February 2025).
42. Zhang, P.; Qiu, H.; Xu, C.; Chen, X.; Zhou, Q. Analysis of the controlling effect of excess topography on the distribution of coseismic landslides during the Iburi earthquake, Japan, on 6 September 2018. *Remote Sens.* **2023**, *15*, 5035. [CrossRef]
43. Pike, R.J.; Wilson, S.E. Elevation-relief ratio, hypsometric integral, and geomorphic area-altitude analysis. *Geol. Soc. Am. Bull.* **1971**, *82*, 1079–1084. [CrossRef]
44. Faul, F.; Erdfelder, E.; Lang, A.-G.; Buchner, A. G* Power 3: A flexible statistical power analysis program for the social, behavioral, and biomedical sciences. *Behav. Res. Methods* **2007**, *39*, 175–191. [CrossRef]
45. Edward, K.A.; Nicholas, P. *Active Tectonics: Earthquakes, Uplift, and Landscape*; Prentice-Hall: Upper Saddle River, NJ, USA, 2002.
46. Hovius, N.; Stark, C.P.; Allen, P.A. Sediment flux from a mountain belt derived by landslide mapping. *Geology* **1997**, *25*, 231–234.
47. Malamud, B.D.; Turcotte, D.L.; Guzzetti, F.; Reichenbach, P. Landslides, earthquakes, and erosion. *Earth Planet. Sci. Lett.* **2004**, *229*, 45–59.
48. Stark, C.P.; Hovius, N. The characterization of landslide size distributions. *Geophys. Res. Lett.* **2001**, *28*, 1091–1094.
49. Çellek, S. Morphological parameters causing landslides: A case study of elevation. *Bull. Miner. Res. Explor.* **2020**, *162*, 197–224.
50. Nalgire, T.; Dahale, P.; Mehta, A.; Hiwase, P. Slope stability analysis by GeoSlope. *Helix* **2020**, *10*, 71–75.
51. Whipple, K.X. Bedrock rivers and the geomorphology of active orogens. *Annu. Rev. Earth Planet. Sci.* **2004**, *32*, 151–185. [CrossRef]
52. Snyder, N.P.; Whipple, K.X.; Tucker, G.E.; Merritts, D.J. Landscape response to tectonic forcing: Digital elevation model analysis of stream profiles in the Mendocino triple junction region, northern California. *Geol. Soc. Am. Bull.* **2000**, *112*, 1250–1263.

Disclaimer/Publisher's Note: The statements, opinions and data contained in all publications are solely those of the individual author(s) and contributor(s) and not of MDPI and/or the editor(s). MDPI and/or the editor(s) disclaim responsibility for any injury to people or property resulting from any ideas, methods, instructions or products referred to in the content.